Supporting Information for:

Evolutionarily Conserved Allosteric Communication in Protein Tyrosine Phosphatases

Michael K. Hjortness,[†] Laura Riccardi,[‡] Akarawin Hongdusit,[†] Peter H. Zwart,[§] Banumathi Sankaran,[§] Marco De Vivo,[‡] and Jerome M. Fox*[,†]

[†]Department of Chemical and Biological Engineering, University of Colorado, 3415 Colorado Avenue, Boulder, Colorado 80303, United States

[‡]Laboratory of Molecular Modeling and Drug Discovery, Istituto Italiano di Tecnologia, Via Morego 30, 16163 Genova, Italy

[§]Molecular Biophysics and Integrated Bioimaging, Lawrence Berkeley National Laboratory, Berkeley, California 94720, United States

SI Methods

Analysis of Residue-Residue Coevolution. We examined the coevolution of residue-residue pairs in the PTP family by using the GREMLIN pseudolikelihood method. In brief, we used an online server (http://gremlin.bakerlab.org/) that (i) generates a multiple sequence alignment (HHBlits, e-value of 1E-10, 4 iterations, UniProt database) from $PTP1B_{1\text{-}321}$, our starting sequence, (ii) filters that alignment by removing sequences that cover less than 75% of the starting sequence and/or that contain over 75% gaps, and (iii) uses the GREMLIN pseudolikelihood method to identify coupled residue-residue pairs. Several recent publications detail the development and use of the GREMLIN approach.[1–3] Figure S2 and Table S3B provide the results of our analysis, and SI Note 1 discusses those results.

SI Notes

SI Note 1. Analysis of Residue-Residue Coevolution. GREMLIN is one of several recently developed approaches for examining residue-residue coevolution in proteins. It differs from SCA by using a pseudolikelihood framework to integrate sequence information and structural context (i.e., crystallographically informed estimates of the likelihood of specific inter-residue contacts[2]). Previous studies suggest that the vast majority of GREMLIN-predicted residue pairs make intra- and intermolecular contact within (or between) proteins and are, thus, poor indicators of the presence of allosteric networks (i.e., regions in which more distally separated pairs might co-evolve[1,3]). We hypothesized, however, that an allosteric network that is conserved across a protein family, and that functions through inter-residue contacts, should manifest itself through clusters of coevolving contacts. Accordingly, we used GREMLIN to look for these contacts; in doing so, we found clusters of interconnected pairs located within (and between) sectors A and B (Figs. S3A and S3D). Some of these pairs showed large separation distances (> 5 Å, a conservative threshold for inter-residue contact), but a comparison of two ligand-bound and ligand-free crystal structures suggests that these distances are probably shorter in alternative conformations of PTP1B (Figs. S3B-S3C and Table S3B). In summary, the high density of co-evolving pairs of contacting residues located within sectors A and B is consistent with their allosteric functionality.

SI Note 2. Results of Comparisons of Kinetic Models. Kinetic data for BBR-mediated inhibition of PTP1B and TC-PTP fit well to mixed models of inhibition, while analogous data for SHP2 fit best to a noncompetitive model (Table S4); these results suggest that the interaction between SHP2 and BBR is insensitive to the presence of bound pNPP.

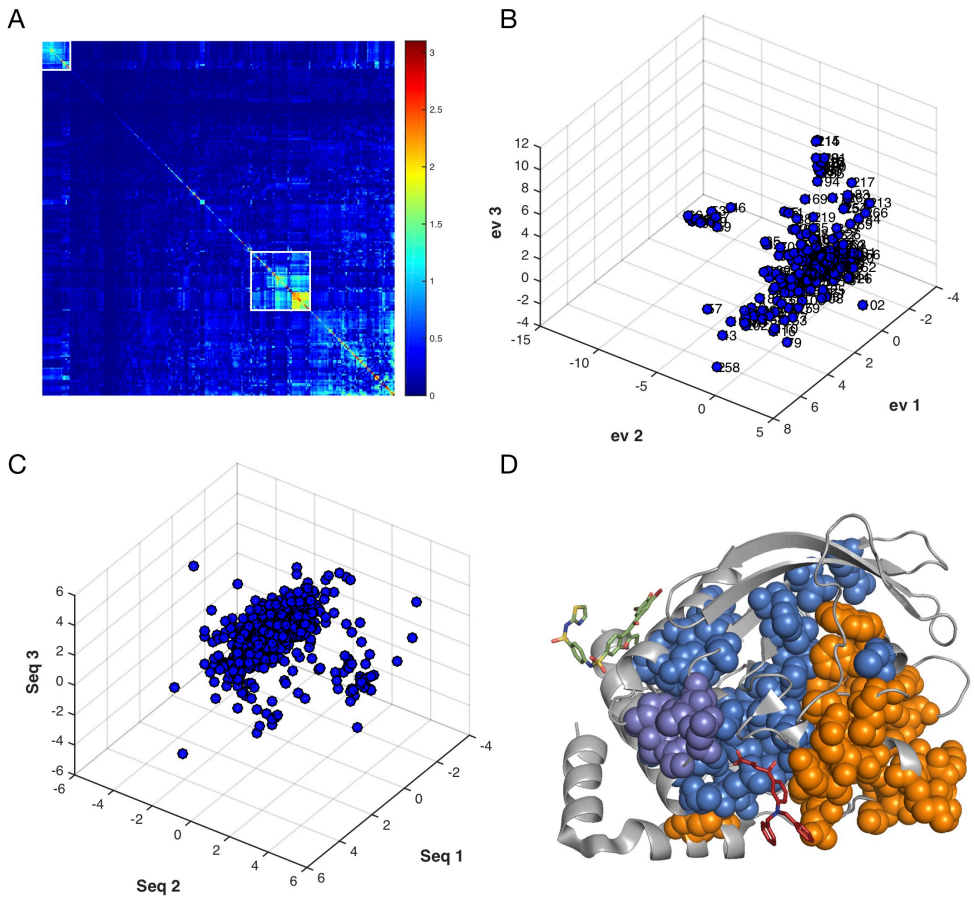

Figure S1. Statistical coupling analysis of PTPs. (A) Hierarchical clustering of the positional correlation matrix shows two groups of positions with strong intragroup correlations. (B) A plot of the first three independent components of this matrix. Two clusters of points, each dominated by positions from one of the two hierarchically clustered groups, appear at extremes of the ev2 and ev3 axes (the left and top, respectively). (C) A mapping of the top three independent components of the positional correlation matrix onto sequence space. Clusters of correlated positions do not map to clusters of correlated sequences; accordingly, positional sectors do not appear to emerge within phylogenetically distinct subfamilies of PTPs. (D) A crystal structure of PTP1B (PDB entry 3A5J) shows sectors A (blue, ev3) and B (orange, ev2) defined as described in the Experimental Section. Inhibitors mark the active site (red, 3EB1) and allosteric site (green, 1T4J); residues from sector A located within the WPD loop are colored purple for reference.

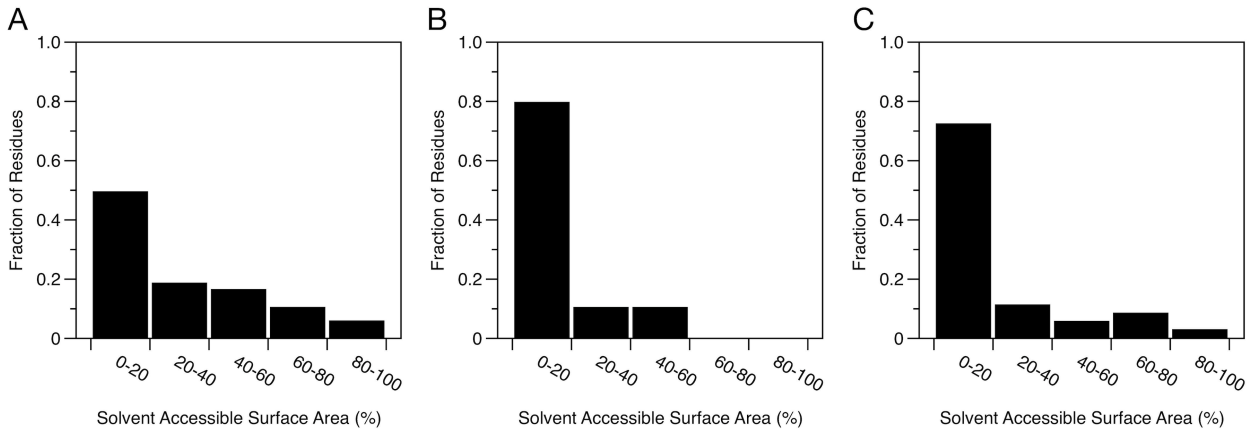

Figure S2. Analysis of solvent exposure. These histograms show the fraction of residues in (A) the full catalytic domain, (B) sector A, and (C) sector B grouped by relative solvent accessible surface area (PyMol, get_sasa_relative, dot_density = 4, solvent_radius = 1.4). (We note: for these analyses, we used the apo structure of PTP1B, or PDB entry 3A5J, as a reference). Distributions from sectors A and B differ from that of PTP1B ($P < 0.01$); the two sectors possess a greater fraction of buried residues.

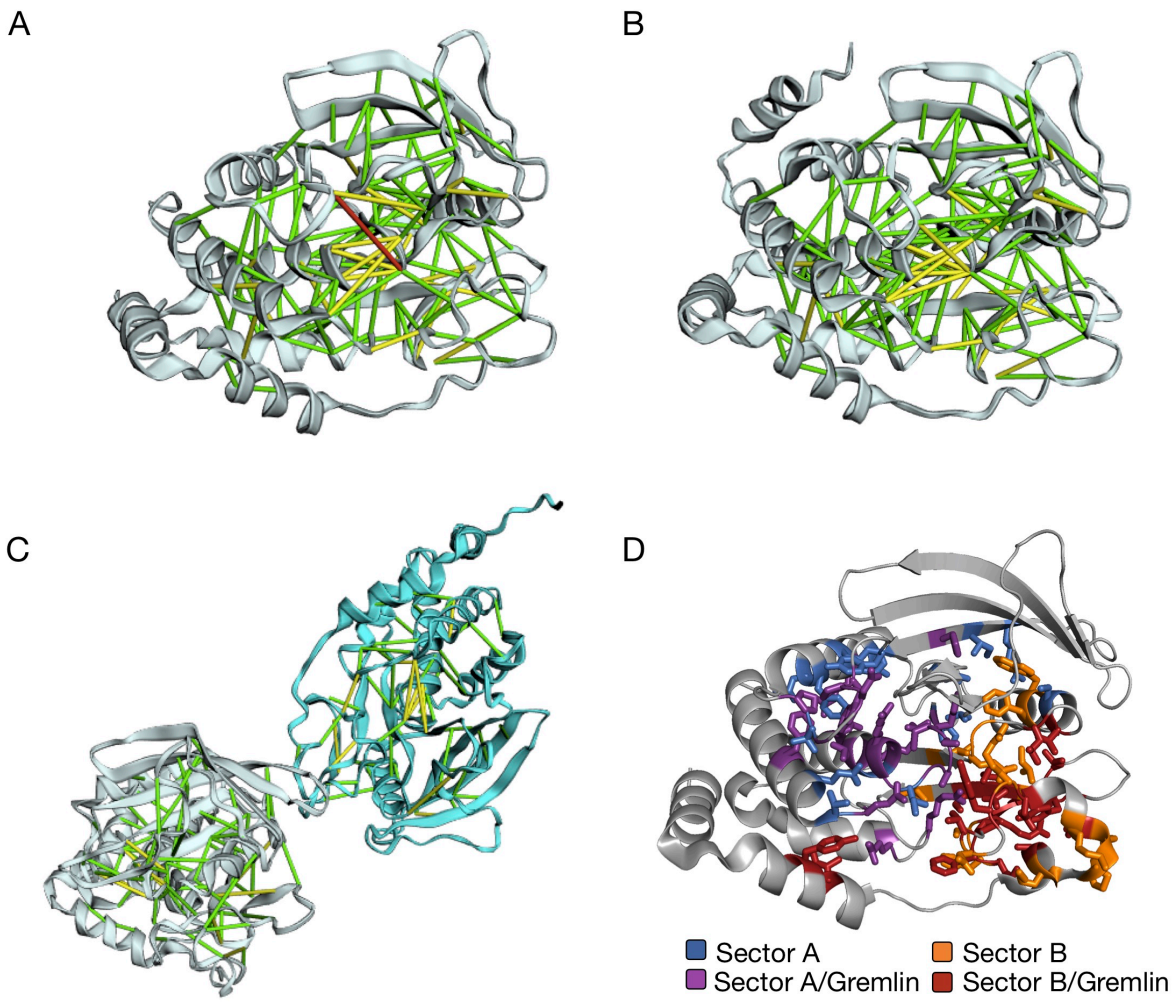

Figure S3. Analysis of residue-residue coevolution in PTPs. (A-C) Pairs of co-evolving residues identified with the GREMLIN pseudolikelihood method are mapped onto three structures of PTP1B: (A) ligand-free (PDB entry 3A5J), (B) competitively inhibited (2F71), and (C) homooligomeric (4BJO). Lines connect pairs of residues with GREMLIN scores larger than 1.0 and inter-residue distances of < 5 Å (green), 5-10 Å (yellow), or > 10 Å (red). (D) A crystal structure of PTP1B (3A5J) highlights GREMLIN-based pairs located entirely within one of the two sectors identified with SCA.

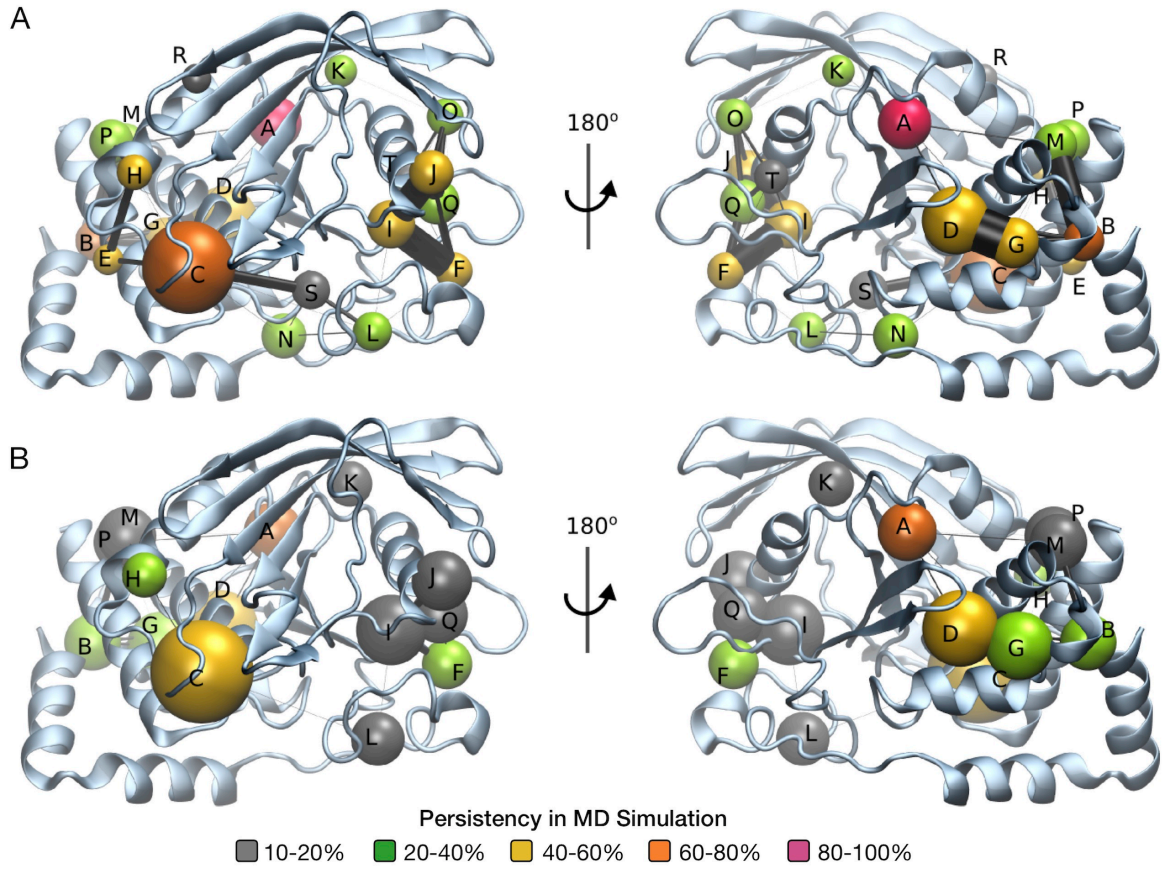

Figure S4. Inter-pocket crosstalk in PTP1B**.** (A) An analysis of crosstalk between pockets sufficient to hold at least three molecules of water. Pockets are represented as spheres, colored according to their persistency along the MD trajectory; the size of each sphere is proportional to its average volume in MD simulations. Lines denote inter-pocket communication and have thicknesses is proportional to the frequency of merging and splitting events.[4] The interconnected networks P-H-E-C-S and F-I-L-N-S include residues from sectors A and B, respectively. (B) An analysis of crosstalk between pockets sufficient to hold at least five molecules of water. Six small pockets from the first analysis disappear: E, O, R, and T, which do not contain sector residues; N, which contains only one sector residue; and S, a pocket defined by two residues from each sector. Tables S3C and S3D list residues associated with each pocket in A and B.

Michaelis-Menten Kinetics

$$[E] + [S] \overset{k_1, k_{-1}}{\longleftrightarrow} [ES] \overset{k_{cat}}{\longrightarrow} [E] + [P]$$

$$K_M = \frac{k_{-1} + k_{cat}}{k_1}$$

One-parameter models:

Competitive:

$$[E] + [I] \overset{K_I}{\leftrightarrow} [EI]$$

Uncompetitive

$$[ES] + [I] \overset{K_I}{\leftrightarrow} [ESI]$$

Noncompetitive:

$$[E] + [I] \overset{K_I}{\leftrightarrow} [EI]$$

$$[ES] + [I] \overset{K_I}{\leftrightarrow} [ESI]$$

Two-parameter model:

Mixed:

$$[E] + [I] \overset{K_{I,c}}{\leftrightarrow} [EI]$$

$$[ES] + [I] \overset{K_{I,u}}{\leftrightarrow} [ESI]$$

Figure S5. Kinetic models. For each PTP, we evaluated four different models of BBR-mediated inhibition. Abbreviations are as follows: enzyme (E), substrate (S), enzyme-substrate complex (ES), enzyme-inhibitor complex (EI), and enzyme-substrate-inhibitor complex (ESI).

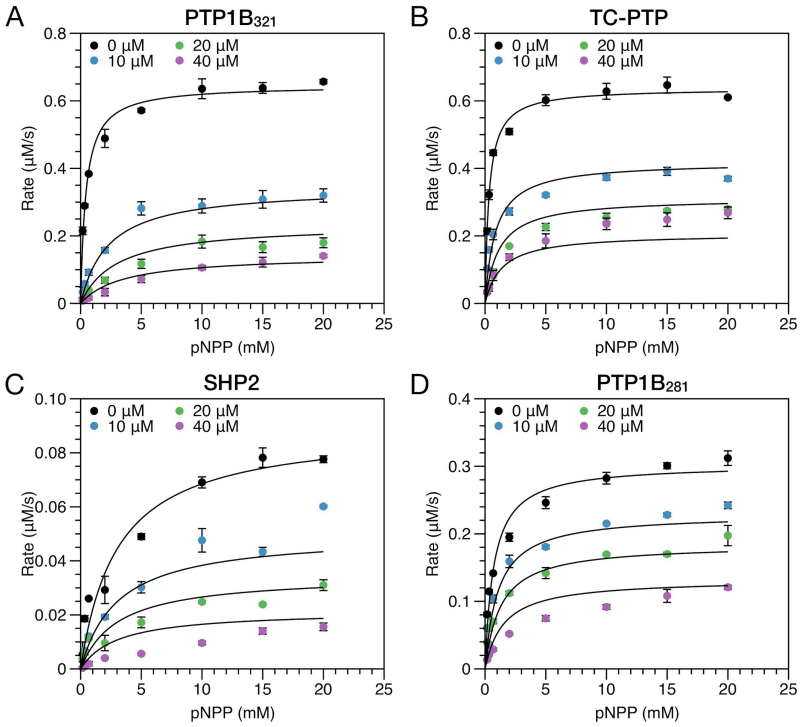

Figure S6. Allosteric inhibition of PTPs. Initial rates of PTP-catalyzed hydrolysis of pNPP in the presence of increasing concentrations of BBR. Lines show models of best fit as follows: (A) $PTP1B_{1\text{-}321}$, mixed; (B) $TC\text{-}PTP_{1\text{-}292}$, mixed; (C) $SHP2_{237\text{-}529}$, noncompetitive; (D) $PTP1B_{1\text{-}281}$, mixed. Error bars denote SE ($n \geq 3$ independent reactions). Exact sample sizes are reported in Table S1B.

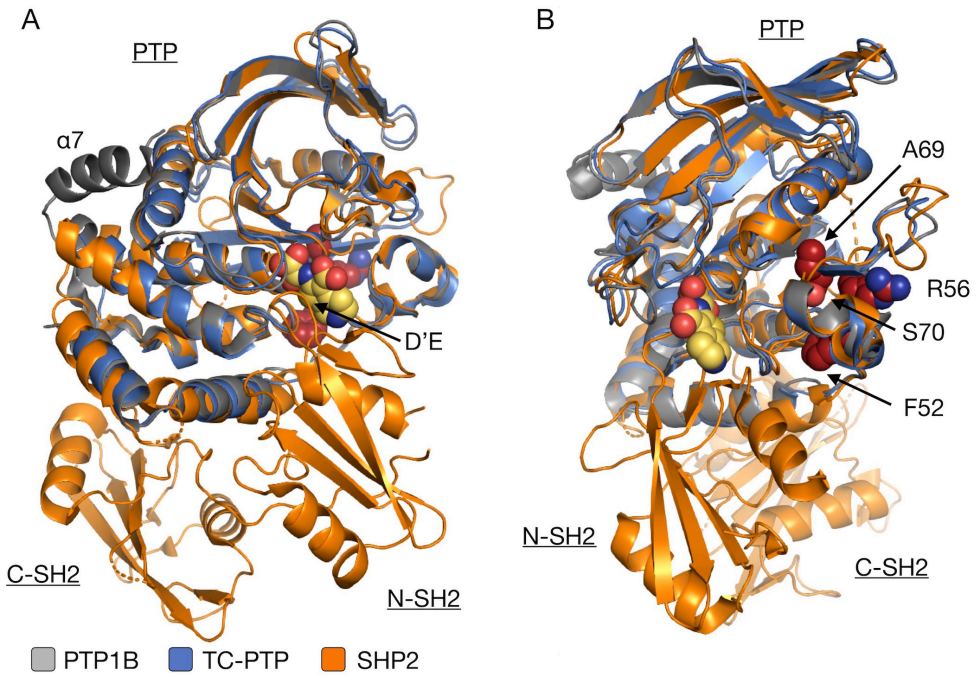

Figure S7. Analysis of functionally influential mutations in sector B. (A) An alignment of PTP1B (PDB entry 5k9W), TC-PTP (1L8K), and SHP2 (5EHR) with the active site (yellow inhibitor, TCS401, 5k9W) highlighted for reference. In autoinhibited SHP2, the D'E loop of the N-SH2 domain blocks the active site; activation occurs when the N-SH2 domain binds a peptide and, upon doing so, undergoes an allosteric conformational change that propagates to the N-SH2/PTP interface to expose the active site.[37] (B) The locations of functionally influential mutations in sector B (labeled for PTP1B). These influential residues appear far (~13-17 Å) from the active site and, thus, likely affect its activity through allosteric communication (here, we used the bound position of TCS401 to determine the position of the active site). For SHP2, allosteric conformational changes may also affect the stability of the N-SH2/PTP interface (which includes part of the active site) and, thus, the equilibrium between open and closed conformations.

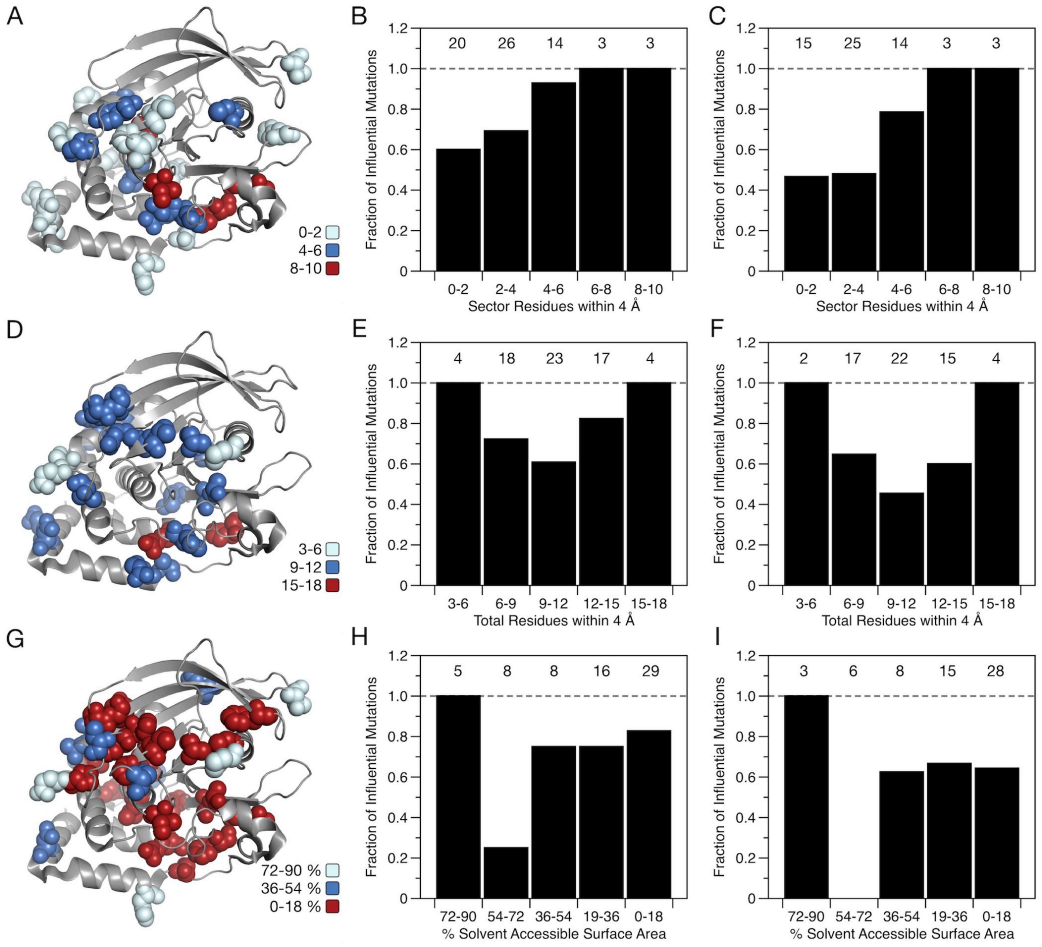

Figure S8. Analysis of experimentally characterized mutations. (A) Mutated sites grouped by the number of sector residues within 4 Å of each. (B-C) The fraction of influential mutations within different groups; here, we define "influential" mutations as those with a significant impact on (B) enzyme kinetics and/or susceptibility to inhibition or (C) only enzyme kinetics. (D) Mutated sites grouped by the number of total residues within 4 Å of each. (E-F) The fraction of mutations that influence (E) enzyme kinetics and/or susceptibility to inhibition or (F) only enzyme kinetics. (G) Mutated sites grouped by their relative solvent accessible surface areas (PyMol, get_sasa_ relative, dot_density = 4, solvent_radius = 1.4). (H-I) The fraction of mutations that influence (H) enzyme kinetics and/or susceptibility to inhibition and (I) only enzyme kinetics. Only the grouping from A-C shows an obvious trend from left to right: residues proximal to sector residues tend to influence function. Sample sizes appear at the top of each plot.

Table S1A. Analysis of Mutants of PTPs

Enzyme	k_{cat} [s^{-1}]	Δk_{cat} [%]**	K_M [μM]	ΔK_M [%]**
PTP1B (WT)*	9.2 (0.5)	NA	282 (89)	NA
PTP1B (C92A)*	5.7 (0.4)	-38 (8)	217 (86)	-23 (44)
PTP1B (M109A)*	1.2 (0.2)	-87 (8)	268 (210)	-5 (81)
PTP1B (R112A)*	10.1 (0.4)	11 (7)	185 (43)	-34 (37)
PTP1B (V113T)*	9.0 (0.4)	-2 (7)	241 (57)	-14 (38)
PTP1B (A122F)*	5.5 (0.3)	-40 (7)	273 (92)	-3 (45)
PTP1B (A122S)*	8.8 (0.4)	-4 (7)	227 (68)	-19 (40)
PTP1B (F135Y)*	10.8 (0.5)	18 (8)	392 (86)	39 (46)
PTP1B (Y152A/Y153A)*	7.1 (0.7)	-22 (10)	396 (211)	41 (82)
PTP1B (H175A)*	5.8 (0.2)	-37 (7)	262 (60)	-7 (38)
PTP1B (F182Y)*	4.0 (0.2)	-56 (7)	275 (64)	-2 (39)
PTP1B (A189S)*	5.0 (0.5)	-45 (8)	330 (177)	17 (71)
PTP1B (F196Y)*	13.1 (0.7)	43 (10)	366 (108)	30 (50)
PTP1B (I219T)*	0.8 (0.1)	-91 (8)	3735 (1121)	1224 (555)
PTP1B (R254A)*	0.4 (0.1)	-95 (8)	2696 (1952)	856 (744)
PTP1B (G259S)*	4.3 (0.3)	-53 (7)	587 (229)	108 (94)
PTP1B (F280Y)*	8.5 (0.5)	-7 (8)	343 (103)	21 (49)
PTP1B (R56G)	1.9 (0.1)	-79 (7)	2930 (540)	939 (354)
TC-PTP (WT)	8.6 (0.3)	NA	209 (42)	NA
TC-PTP (A71V)	3.0 (0.3)	-66 (5)	224 (119)	7 (60)

*Newly collected kinetic measurements of mutations developed in Hjortness et al.[5]
**Values of Δk_{cat} and ΔK_M correspond to differences between kinetic parameters for mutant and wild-type enzymes.
***For all measurements, values in parentheses indicate the 95% confidence interval.

Table S1B. Discrete Kinetic Measurements of PTPs and Mutants.
This table details the discrete kinetic measurements made in this study, including standard error and exact sample sizes. See the Excel file that accompanies this work.

Table S2. Crystallographic Data for Mutants of PTP1B.

	A122S	***F135Y***
Accession code (www.rcsb.org)	6CWV	6CWU
No. crystals analyzed	1	1
Wavelength	Å	Å
Space group	$P3_121$	$P3_121$
Unit cell parameters		
a	89.43	89.20
b	89.43	89.20
c	105.55	105.73
α	90.00	90.00
β	90.00	90.00
γ	120.00	120.00
Diffraction data		
High resolution bin	2.04-1.98	2.13-2.08
# of reflections	2612	1961
Refinement		
Resolution range	44.72-1.98	77.25-2.08
Completeness	99.3	95.98
R(work)	0.2046	0.2547
R(free)	0.2464	0.2912
B(avg)	39.2	39.1
Bond lengths	0.008	0.006
Bond angles	0.818	1.046
Protein residues	281	281
Magnesium ions	1	1
Water molecules*	220	352

*This number denotes the number of water molecules observed in the crystal structure (inside the binding pocket and exterior to the protein).
**Crystal structures are available in the Protein Data Bank (www.rcsb.org).

Table S3A. Results of SCA: Sectors with Strong Intragroup Correlations.

Sector A	*Sector B*
92, 107, **169**, **171**, 173, 176, **179**, 180, 181, **183**, **184**, **185**, 191, **192**, 194, 198, 199, **210**, 212, 213, 214, 215, 216, **217**, 218, **219**, 220, **221**, 222, 223, 224, 226, 229, **254**, 257, 262, **263**, **266**, **269**	20, 23, **35**, **36**, 38, 39, **40**, **41**, **44**, 45, **46**, 48, **49**, 51, **52**, 53, 54, 55, 56, 57, 59, **65**, **66**, **67**, 68, 69, 70, 72, 82, **85**, 86, 88, **91**, 95, 96, 173

*Residues in bold overlap with pockets identified our analysis of inter-pocket crosstalk.

Table S3B. Results of GREMLIN: Spatially Separated Coevolving Residue-Residue Pairs.

Res i	*Res j*	*Score*	*Prob*	*3A5J*	*2F71*	*Diff*	*Res i*	*Res j*	*Score*	*Prob*	*3A5J*	*2F71*	*Diff*
71	102	1.905	1	6.1	6.08	0.02	86	111	1.084	0.99	5.77	5.57	0.2
181	217	1.89	1	12.71	6.45	6.26	226	260	1.053	0.99	6.42	5.83	0.59
228	270	1.746	1	5.02	4.85	0.17	250	270	1.049	0.99	6.84	6.31	0.53
217	221	1.74	1	7.25	6.61	0.64	217	222	1.038	0.98	6.01	6.05	0.04
119	122	1.71	1	6.25	6.02	0.23	266	271	1.015	0.98	5.21	5.25	0.04
217	220	1.604	1	5.6	5.56	0.04							
56	59	1.6	1	5.59	5.62	0.03							
216	221	1.483	1	6.3	3.08	3.22							
218	221	1.464	1	6.16	6.07	0.09							
106	174	1.279	1	5.09	4.51	0.58							
89	119	1.27	1	7.05	7.39	0.34							
59	69	1.241	1	7.47	7.47	0							
66	69	1.205	0.99	5.39	5.38	0.01							
52	68	1.193	0.99	7.24	7.28	0.04							
216	220	1.184	0.99	6.9	6.96	0.06							
40	53	1.159	0.99	8.11	8.11	0							
247	267	1.154	0.99	5.83	5.36	0.47							
216	262	1.151	0.99	6.87	9.39	2.52							
143	161	1.145	0.99	6.17	6.29	0.12							
51	258	1.119	0.99	5.46	5.45	0.01							
120	181	1.103	0.99	8.47	2.51	5.96							

*Highlights. Blue: pairs of residues that exist entirely within one of the two SCA-based sectors. Green through red: residues separated by < 5 Å (green), 5-10 Å (yellow), or > 10 Å (red).

Table S3C. Analysis of Inter-Pocket Crosstalk (Pocket Size ≥ 3 Water Molecules)

Pocket ID	*Persistency (% MD simulation)*	*Residues ≥ 80% of the Time*	*Avg Volume (Å^3)*
A	91	204, **210**, 79, 80, 206, 205, 208, 209	96
B	61	3, 2, 242, 244	74
C	60	**183**, **266**, **263**, 182, 265, **179**, **221**, **184**	167
D	55	74, 252, 76, 234, 75, 249	122
E	53	268, **269**, 272, **184**, **185**, 186	55
F	52	**40**, 39, 63, **65**, 64, **66**, 37	67
G	46	249, 248, 238, 244, 245, 234, 243	91
H	45	190, **185**, 187, 152, 178, 186	64
I	40	**67**, **91**, **85**, 43, 87	87
J	40	90, 93, 137, 135	80
K	39	**169**, 103, 104, 105, **171**, 170	58
L	34	47, **41**, 50, **44**, **36**, **35**	70
M	30	236, 232, 281	79
N	23	**254**, 27, 28, 258, **52**, 29, 259	81
O	22	97, 162, 138, 140, 60, 139	66
P	22	196, 280, **192**	79
Q	16	94, 61, 64	81
R	15	155, 148, 197, 153, 150	53
S	13	**46**, **49**, **217**, **219**	69
T	11	59, 60, 97, 101	62

*See Figure S3A for the pocket ID reference.
**Residues that overlap with SCA-based sectors are highlighted in blue (sector A) and orange (sector B).

Table S3D. Analysis of Inter-Pocket Crosstalk (Pocket Size ≥ 5 Water Molecules)

Pocket ID	*Persistency (% MD simulation)*	*Residues ≥ 80% of the Time*	*Avg Volume (Å^3)*
A	74	204, **210**, 79, 80, 206, 205, 208, 209, 78	105
B	30	3, 2, 242, 244, 241, 235, 1	101
C	54	**183**, **266**, **263**, 182, 181, **216**, **179**, **221**	185
D	46	74, 252, 76, 234, 75, 249	137
E	10	268, **269**, 272, **184**, **185**, 186	82
F	24	**40**, 39, 63, **65**, 64, **66**, 37	90
G	26	249, 248, 238, 244, 245, 234, 243, 74, 76, 252	122
H	20	190, **185**, 187, 152, 178, 186	81
I	19	**67**, **91**, **85**, 43, 87, 94, **95**, **68**	126
J	19	90, 93, 137, 135, 94, 138	108
K	10	**169**, 103, 104, 105, **171**, 170, 99	82
L	15	47, **41**, 50, **44**, **36**, **35**	96
M	18	236, 232, 281, 278, **199**, 135	102
P	14	196, 280	105
Q	16	94	102

*See Figure S3B for the pocket ID reference.
**Residues in blue (sector A) and orange (sector B) overlap with SCA-based sectors.
***Underlined residues are new, relative to the first analysis.

Table S4A. Comparison of Kinetic Models for the Inhibition of $PTP1B_{1-321}$ by BBR.

Model	*SSE ($\mu M^2/s^2$)*	*DF*	*Criteria*	*Reference*	*Fit Param. (μM)*
Competitive	0.0493	35			Ki = 0.298
Uncompetitive	0.104	35			Ki = 5.53
Noncompetitive	0.0499	35			Ki = 6.73
Mixed	0.0114	34	$p < 0.001$	Competitive and Noncompetitive	Kic = 1.12 Kiu = 11.4

Table S4B. Comparison of Kinetic Models for the Inhibition of TC-PTP_{1-292} by BBR.

Model	*SSE ($\mu M^2/s^2$)*	*DF*	*Criteria*	*Reference*	*Fit Param. (μM)*
Competitive	0.136	35			Ki = 0.566
Uncompetitive	0.115	35			Ki = 12.0
Noncompetitive	0.0589	35			Ki = 13.8
Mixed	0.0263	34	$p < 0.001$	Noncompetitive	Kic = 3.42 Kiu = 19.2

Table S4C. Comparison of Kinetic Models for the Inhibition of $SHP2_{237-529}$ by BBR.

Model	*SSE ($\mu M^2/s^2$)*	*DF*	*Criteria*	*Reference*	*Fit Param. (μM)*
Competitive	0.00117	35	$\Delta_i = 8.20$	Noncompetitive	Ki = 2.52
Uncompetitive	0.00133	35	$\Delta_i = 12.7$	Noncompetitive	Ki = 9.30
Noncompetitive	0.00093	35			Ki = 12.7
Mixed	0.00089	34	$p = 0.209$	Noncompetitive	Kic = 7.15 Kiu = 16.5

Table S4D. Comparison of Kinetic Models for the Inhibition of $PTP1B_{1-281}$ by BBR.

Model	*SSE ($\mu M^2/s^2$)*	*DF*	*Criteria*	*Reference*	*Fit Param. (μM)*
Competitive	0.0297	35			Ki = 2.05
Uncompetitive	0.0196	35			Ki = 21.6
Noncompetitive	0.0109	35			Ki = 25.1
Mixed	0.00854	34	$p = 0.004$	Noncompetitive	Kic = 10.4 Kiu = 31.1

* Blue highlights indicate models of best fit.

Table S5A. Analysis of Experimentally Characterized Pathologically Relevant Mutations.
This table lists experimentally characterized mutations from previous studies and analyzes them as described in the Experimental Section. See the Excel file that accompanies this work.[5-36]

Table S5B. Analysis of Disease-Associated Mutations.
This table lists disease-associated mutations from previous studies and analyzes them as described in the Experimental Section. See the Excel file that accompanies this work.[5-36]

SI References

(1) Anishchenko, I., Ovchinnikov, S., Kamisetty, H., and Baker, D. (2017) Origins of coevolution between residues distant in protein 3D structures. *Proc. Natl. Acad. Sci.* 201702664.

(2) Kamisetty, H., Ovchinnikov, S., and Baker, D. (2013) Assessing the utility of coevolution-based residue-residue contact predictions in a sequence- and structure-rich era. *Proc. Natl. Acad. Sci. 110*, 15674–15679.

(3) Ovchinnikov, S., Kamisetty, H., and Baker, D. (2014) Robust and accurate prediction of residue-residue interactions across protein interfaces using evolutionary information. *Elife 2014*.

(4) La Sala, G., Decherchi, S., De Vivo, M., and Rocchia, W. (2017) Allosteric Communication Networks in Proteins Revealed through Pocket Crosstalk Analysis. *ACS Cent. Sci.* acscentsci.7b00211.

(5) Hjortness, M. K., Riccardi, L., Hongdusit, A., Ruppe, A., Zhao, M., Kim, E. Y., Zwart, P. H., Sankaran, B., Arthanari, H., Sousa, M. C., De Vivo, M., and Fox, J. M. (2018) Abietane-Type Diterpenoids Inhibit Protein Tyrosine Phosphatases by Stabilizing an Inactive Enzyme Conformation. *Biochemistry*. DOI: acs.biochem.8b00655.

(6) Villa, F., Deak, M., Bloomberg, G. B., Alessi, D. E., and Van Aalten, D. M. F. (2005) Crystal structure of the PTPL1/FAP-1 human tyrosine phosphatase mutated in colorectal cancer: Evidence for a second phosphotyrosine substrate recognition pocket. *J. Biol. Chem. 280*, 8180–8187.

(7) Tartaglia, M., Mehler, E. L., Goldberg, R., Zampino, G., Brunner, H. G., Kremer, H., van der Burgt, I., Crosby, a H., Ion, A., Jeffery, S., Kalidas, K., Patton, M. a, Kucherlapati, R. S., and Gelb, B. D. (2001) Mutations in PTPN11, encoding the protein tyrosine phosphatase SHP-2, cause Noonan syndrome. *Nat. Genet. 29*, 465–8.

(8) Solomon, D. A., Kim, J. S., Cronin, J. C., Sibenaller, Z., Ryken, T., Rosenberg, S. A., Ressom, H., Jean, W., Bigner, D., Yan, H., Samuels, Y., and Waldman, T. (2008) Mutational inactivation of PTPRD in glioblastoma multiforme and malignant melanoma. *Cancer Res. 68*, 10300–10306.

(9) Hoover, A. C., Strand, G. L., Nowicki, P. N., Anderson, M. E., Vermeer, P. D., Klingelhutz, A. J., Bossler, A. D., Pottala, J. V., Hendriks, W. J. A. J., and Lee, J. H. (2009) Impaired PTPN13 phosphatase activity in spontaneous or HPV-induced squamous cell carcinomas potentiates oncogene signaling through the MAP kinase pathway. *Oncogene 28*, 3960–3970.

(10) Sun, T., Aceto, N., Meerbrey, K. L., Kessler, J. D., Zhou, C., Migliaccio, I., Nguyen, D. X., Pavlova, N. N., Botero, M., Huang, J., Bernardi, R. J., Schmitt, E., Hu, G., Li, M. Z., Dephoure, N., Gygi, S. P., Rao, M., Creighton, C. J., Hilsenbeck, S. G., Shaw, C. A., Muzny, D., Gibbs, R. A., Wheeler, D. A., Osborne, C. K., Schiff, R., Bentires-Alj, M., Elledge, S. J., and Westbrook, T. F. (2011) Activation of multiple proto-oncogenic tyrosine kinases in breast cancer via loss of the PTPN12 phosphatase. *Cell 144*, 703–718.

(11) Kleppe, M., Tousseyn, T., Geissinger, E., Atak, Z. K., Aerts, S., Rosenwald, A., Wlodarska, I., and Cools, J. (2011) Mutation analysis of the tyrosine phosphatase PTPN2 in Hodgkin's lymphoma and T-cell non-Hodgkin's lymphoma. *Haematologica 96*, 1723–1727.

(12) Stransky, N., Egloff, A. M., Tward, A. D., Kostic, A. D., Cibulskis, K., Sivachenko, A., Kryukov, G. V, Lawrence, M. S., Sougnez, C., McKenna, A., Shefler, E., Ramos, A. H., Stojanov, P., Carter, S. L., Voet, D., Cortés, M. L., Auclair, D., Berger, M. F., Saksena, G., Guiducci, C., Onofrio, R. C., Parkin, M., Romkes, M., Weissfeld, J. L., Seethala, R. R., Wang, L., Rangel-Escareño, C., Fernandez-Lopez, J. C., Hidalgo-Miranda, A., Melendez-Zajgla, J., Winckler, W., Ardlie, K., Gabriel, S. B., Meyerson, M., Lander, E. S., Getz, G., Golub, T. R.,

Garraway, L. a, and Grandis, J. R. (2011) The mutational landscape of head and neck squamous cell carcinoma. *Science 333*, 1157–60.

(13) Porcu, M., Kleppe, M., Gianfelici, V., Geerdens, E., De Keersmaecker, K., Tartaglia, M., Foà, R., Soulier, J., Cauwelier, B., Uyttebroeck, A., MacIntyre, E., Vandenberghe, P., Asnafi, V., and Cools, J. (2012) Mutation of the receptor tyrosine phosphatase PTPRC (CD45) in T-cell acute lymphoblastic leukemia. *Blood 119*, 4476–4479.

(14) Lauriol, J., and Kontaridis, M. I. (2011) PTPN11-Associated Mutations in the Heart: Has LEOPARD Changed Its RASpots? *Trends Cardiovasc. Med.*

(15) Agarwal, S., Al-Keilani, M. S., Alqudah, M. A. Y., Sibenaller, Z. A., Ryken, T. C., and Assem, M. (2013) Tumor Derived Mutations of Protein Tyrosine Phosphatase Receptor Type K Affect Its Function and Alter Sensitivity to Chemotherapeutics in Glioma. *PLoS One 8*.

(16) Yu, K. R., Kim, Y. J., Jung, S. K., Ku, B., Park, H., Cho, S. Y., Jung, H., Chung, S. J., Bae, K. H., Lee, S. C., Kim, B. Y., Erikson, R. L., Ryu, S. E., and Kim, S. J. (2013) Structural basis for the dephosphorylating activity of PTPRQ towards phosphatidylinositide substrates. *Acta Crystallogr. Sect. D Biol. Crystallogr. 69*, 1522–1529.

(17) Lui, V. W. Y., Peyser, N. D., Ng, P. K.-S., Hritz, J., Zeng, Y., Lu, Y., Li, H., Wang, L., Gilbert, B. R., General, I. J., Bahar, I., Ju, Z., Wang, Z., Pendleton, K. P., Xiao, X., Du, Y., Vries, J. K., Hammerman, P. S., Garraway, L. A., Mills, G. B., Johnson, D. E., and Grandis, J. R. (2014) Frequent mutation of receptor protein tyrosine phosphatases provides a mechanism for STAT3 hyperactivation in head and neck cancer. *Proc. Natl. Acad. Sci. 111*, 1114–1119.

(18) Wang, Z., Shen, D., Parsons, D. W., Bardelli, A., Sager, J., Szabo, S., Ptak, J., Silliman, N., Peters, B. A., Van Der Heidjden, M. S., Parmigiani, G., Yan, H., Wang, T. L., Riggins, G., Powell, S. M., Willson, J. K. V., Markowitz, S., Kinzler, K. W., Vogelstein, B., and Velculescu, V. E. (2004) Mutational analysis of the tyrosine phosphatome in colorectal cancers. *Science. 304*, 1164–1166.

(19) Gunawardana, J., Chan, F. C., Telenius, A., Woolcock, B., Kridel, R., Tan, K. L., Ben-Neriah, S., Mottok, A., Lim, R. S., Boyle, M., Rogic, S., Rimsza, L. M., Guiter, C., Leroy, K., Gaulard, P., Haioun, C., Marra, M. A., Savage, K. J., Connors, J. M., Shah, S. P., Gascoyne, R. D., and Steidl, C. (2014) Recurrent somatic mutations of PTPN1 in primary mediastinal B cell lymphoma and Hodgkin lymphoma. *Nat. Genet. 46*, 329–335.

(20) Behjati, S., Tarpey, P. S., Sheldon, H., Martincorena, I., Van Loo, P., Gundem, G., Wedge, D. C., Ramakrishna, M., Cooke, S. L., Pillay, N., Vollan, H. K. M., Papaemmanuil, E., Koss, H., Bunney, T. D., Hardy, C., Joseph, O. R., Martin, S., Mudie, L., Butler, A., Teague, J. W., Patil, M., Steers, G., Cao, Y., Gumbs, C., Ingram, D., Lazar, A. J., Little, L., Mahadeshwar, H., Protopopov, A., Al Sannaa, G. A., Seth, S., Song, X., Tang, J., Zhang, J., Ravi, V., Torres, K. E., Khatri, B., Halai, D., Roxanis, I., Baumhoer, D., Tirabosco, R., Amary, M. F., Boshoff, C., McDermott, U., Katan, M., Stratton, M. R., Futreal, P. A., Flanagan, A. M., Harris, A., and Campbell, P. J. (2014) Recurrent PTPRB and PLCG1 mutations in angiosarcoma. *Nat. Genet. 46*, 376–379.

(21) Wang, H. M., Xu, Y. F., Ning, S. L., Yang, D. X., Li, Y., Du, Y. J., Yang, F., Zhang, Y., Liang, N., Yao, W., Zhang, L. L., Gu, L. C., Gao, C. J., Pang, Q., Chen, Y. X., Xiao, K. H., Ma, R., Yu, X., and Sun, J. P. (2014) The catalytic region and PEST domain of PTPN18 distinctly regulate the HER2 phosphorylation and ubiquitination barcodes. *Cell Res. 24*, 1067–1090.

(22) Walia, V., Prickett, T. D., Kim, J. S., Gartner, J. J., Lin, J. C., Zhou, M., Rosenberg, S. A., Elble, R. C., Solomon, D. A., Waldman, T., and Samuels, Y. (2014) Mutational and functional analysis of the tumor-suppressor PTPRD in human melanoma. *Hum. Mutat. 35*, 1301–1310.

(23) Lemay, P., Guyot, M.-C., Tremblay, É., Dionne-Laporte, A., Spiegelman, D., Henrion, É., Diallo, O., De Marco, P., Merello, E., Massicotte, C., Désilets, V., Michaud, J. L., Rouleau, G. A., Capra, V., and Kibar, Z. (2015) Loss-of-function de novo mutations play an important role in severe human neural tube defects. *J. Med. Genet. 52*, 493–497.

(24) Mulero-Navarro, S., Sevilla, A., Roman, A. C., Lee, D.-F., D'Souza, S. L., Pardo, S., Riess, I., Su, J., Cohen, N., Schaniel, C., Rodriguez, N. A., Baccarini, A., Brown, B. D., Cavé, H., Caye, A., Strullu, M., Yalcin, S., Park, C. Y., Dhandapany, P. S., Yongchao, G., Edelmann, L., Bahieg, S., Raynal, P., Flex, E., Tartaglia, M., Moore, K. A., Lemischka, I. R., and Gelb, B. D. (2015) Myeloid Dysregulation in a Human Induced Pluripotent Stem Cell Model of PTPN11-Associated Juvenile Myelomonocytic Leukemia. *Cell Rep. 13*, 504–515.

(25) Bonilla, X., Parmentier, L., King, B., Bezrukov, F., Kaya, G., Zoete, V., Seplyarskiy, V. B., Sharpe, H. J., McKee, T., Letourneau, A., Ribaux, P. G., Popadin, K., Basset-Seguin, N., Chaabene, R. Ben, Santoni, F. A., Andrianova, M. A., Guipponi, M., Garieri, M., Verdan, C., Grosdemange, K., Sumara, O., Eilers, M., Aifantis, I., Michielin, O., De Sauvage, F. J., Antonarakis, S. E., and Nikolaev, S. I. (2016) Genomic analysis identifies new drivers and progression pathways in skin basal cell carcinoma. *Nat. Genet. 48*, 398–406.

(26) LaRochelle, J. R., Fodor, M., Xu, X., Durzynska, I., Fan, L., Stams, T., Chan, H. M., LaMarche, M. J., Chopra, R., Wang, P., Fortin, P. D., Acker, M. G., and Blacklow, S. C. (2016) Structural and Functional Consequences of Three Cancer-Associated Mutations of the Oncogenic Phosphatase SHP2. *Biochemistry 55*, 2269–2277.

(27) Choy, M. S., Li, Y., Machado, L. E. S. F., Kunze, M. B. A., Connors, C. R., Wei, X., Lindorff-Larson, K., Page, R., and Peti, W. (2017) Conformational Rigidity and Protein Dynamics at Distinct Timescales Regulate PTP1B Activity and Allostery. *Mol. Cell 65*, 644–658.

(28) Li, H., Yang, D., Ning, S., Xu, Y., Yang, F., Yin, R., and Feng, T. (2018) Switching of the substrate specificity of protein tyrosine phosphatase N12 by cyclin-dependent kinase 2 phosphorylation orchestrating 2 oncogenic pathways 73–82.

(29) Bentires-Alj, M., Paez, J. G., David, F. S., Keilhack, H., Halmos, B., Naoki, K., Maris, J. M., Richardson, A., Bardelli, A., Sagarbaker, D. J., Richards, W. G., Du, J., Girard, L., Minna, J. D., Loh, M. L., Fisher, D. E., Velculescu, V. E., Vogelstein, B., Meyerson, M., Sellers, W. R., and Neel, B. G. (2004) Activating mutations of the Noonan syndrome-associated SHP2/PTPN11 gene in human solid tumors and adult acute myelogenous leukemia. *Cancer Res. 64*, 8816–8820.

(30) Sowada, N., Hashem, M. O., Yilmaz, R., Hamad, M., Kakar, N., Thiele, H., Arold, S. T., Bode, H., Alkuraya, F. S., and Borck, G. (2017) Mutations of PTPN23 in developmental and epileptic encephalopathy. *Hum. Genet. 136*, 1455–1461.

(31) Keilhack, H., David, F. S., McGregor, M., Cantley, L. C., and Neel, B. G. (2005) Diverse biochemical properties of Shp2 mutants: Implications for disease phenotypes. *J. Biol. Chem. 280*, 30984–30993.

(32) Montalibet, J., Skorey, K., McKay, D., Scapin, G., Asante-Appiah, E., and Kennedy, B. P. (2006) Residues distant from the active site influence protein-tyrosine phosphatase 1B inhibitor binding. *J. Biol. Chem. 281*, 5258–5266.

(33) Hanna, N., Montagner, A., Lee, W. H., Miteva, M., Vidal, M., Vidaud, M., Parfait, B., and Raynal, P. (2006) Reduced phosphatase activity of SHP-2 in LEOPARD syndrome: Consequences for PI3K binding on Gab1. *FEBS Lett. 580*, 2477–2482.

(34) Weir, B. A., Woo, M. S., Getz, G., Perner, S., Ding, L., Beroukhim, R., Lin, W. M., Province, M. A., Kraja, A., Johnson, L. A., Shah, K., Sato, M., Thomas, R. K., Barletta, J. A., Borecki, I. B., Broderick, S., Chang, A. C., Chiang, D. Y., Chirieac, L. R., Cho, J., Fujii, Y., Gazdar, A. F., Giordano, T., Greulich, H., Hanna, M., Johnson, B. E., Kris, M. G., Lash, A., Lin, L., Lindeman, N., Mardis, E. R., McPherson, J. D., Minna, J. D., Morgan, M. B., Nadel, M., Orringer, M. B., Osborne, J. R., Ozenberger, B., Ramos, A. H., Robinson, J., Roth, J. A., Rusch, V., Sasaki, H., Shepherd, F., Sougnez, C., Spitz, M. R., Tsao, M. S., Twomey, D., Verhaak, R. G. W., Weinstock, G. M., Wheeler, D. A., Winckler, W., Yoshizawa, A., Yu, S., Zakowski, M. F., Zhang, Q., Beer, D. G., Wistuba, I. I., Watson, M. A., Garraway, L. A., Ladanyi, M., Travis, W. D., Pao, W., Rubin, M. A., Gabriel, S. B., Gibbs, R. A., Varmus, H. E., Wilson, R. K., Lander, E. S., and Meyerson, M. (2007) Characterizing the cancer genome in lung adenocarcinoma. *Nature 450*, 893–898.

(35) Zhu, J. H., Chen, R., Yi, W., Cantin, G. T., Fearns, C., Yang, Y., Yates, J. R., and Lee, J. D. (2008) Protein tyrosine phosphatase PTPN13 negatively regulates Her2/ErbB2 malignant signaling. *Oncogene 27*, 2525–2531.

(36) Orrú, V., Tsai, S. J., Rueda, B., Fiorillo, E., Stanford, S. M., Dasgupta, J., Hartiala, J., Zhao, L., Ortego-Centeno, N., D'Alfonso, S., Arnett, F. C., Wu, H., Gonzalez-Gay, M. A., Tsao, B. P., Pons-Estel, B., Alarcon-Riquelme, M. E., He, Y., Zhang, Z. Y., Allayee, H., Chen, X. S., Martin, J., Bottini, N., Danieli, G., Galeazzi, M., Sabbadini, M. G., Migliaresi, S., and Domenico, G. (2009) A loss-of-function variant of PTPN22 is associated with reduced risk of systemic lupus erythematosus. *Hum. Mol. Genet. 18*, 569–579.

(37) Barford, D., and Neel, B. G. (1998) Revealing mechanisms for SH2 domain mediated regulation of the protein tyrosine phosphatase SHP-2. *Structure*.